Case Studies in Construction Materials 20 (2024) e02919

Contents lists available at ScienceDirect

Case Studies in Construction Materials

journal homepage: www.elsevier.com/locate/cscm

Understanding the role of epoxy resin and polyurethane in toughening metakaolin-based geopolymer matrix

Feng Chen [a], Gonghui Gu [a,b,*], Yingqi Shi [c], Fang Xu [d], Tao Ma [a]

[a] School of Transportation, Southeast University, Nanjing 211189, PR China
[b] School of Civil and Environmental Engineering, Nanyang Technological University, Singapore 639798, Singapore
[c] Department of Civil and Environmental Engineering, Imperial College London, London SW7 2AZ, United Kingdom
[d] Faculty of Engineering, China University of Geosciences, Wuhan 430074, PR China

ARTICLE INFO

Keywords:
Epoxy resin
Polyurethane modified epoxy resin
Metakaolin-based geopolymer
Toughening mechanism
Chemical bond evolution

ABSTRACT

Geopolymer is promising to replace cement, thus reducing the CO_2 emissions of concrete production. However, the brittle behavior of geopolymer under bending loads limits its engineering applications. This work adopted epoxy resin and polyurethane modified epoxy resin (PMER) to synthesize the epoxy resin-PMER (EP) emulsion, which was further added into metakaolin-based geopolymer matrix for toughening. Moreover, the co-toughening mechanism of epoxy resin and polyurethane on metakaolin-based geopolymer was revealed based on the changes of major chemical bonds and Si binding energy of geopolymer before and after modification. The results show that the introduction of PMER does contribute to improve the flexural strength of geopolymer matrix by enhancing EP toughness. However, PMER also plays an adverse role in the Si-O-C bond generation of EP-modified metakaolin-based geopolymer (EMG), thus weakening the interconnections between 3D mesh structures inside EMG. A balance between these two contrasting effects is achieved when PMER content within EP reaches 60 wt%. At this time, the addition of 10 wt% EP can increase the flexural strength of metakaolin-based geopolymer matrix by 2.6 times.

1. Introduction

1.1. Background

Cement concrete is a widely used construction material nowadays, whose production will reach 5.5 billion tons per year by 2050 based on the latest reports[1]. During the production process of traditional cement concrete, ordinary Portland cement is adopted as the binder material. It has been reported that approximately 1.7 t non-renewable resources, such as limestone, are consumed in the production of 1 t ordinary Portland cement[2]. In addition, this production process also results in the release of about 1 t CO_2 into the atmosphere due to the high-temperature calcination and subsequent decomposition of calcium carbonate, which leads to the negative environmental effects[3]. Therefore, it is necessary to find a new cementitious material with a low carbon footprint to replace cement as the binder material of concrete, thus reducing the energy consumption and CO_2 emissions in the concrete production.

* Corresponding author at: School of Transportation, Southeast University, Nanjing 211189, PR China.
E-mail addresses: fengc@seu.edu.cn (F. Chen), gugonghui@seu.edu.cn (G. Gu), yingqi.shi23@imperial.ac.uk (Y. Shi), xufang@cug.edu.cn (F. Xu), matao@seu.edu.cn (T. Ma).

https://doi.org/10.1016/j.cscm.2024.e02919
Received 23 October 2023; Received in revised form 10 January 2024; Accepted 24 January 2024
Available online 26 January 2024

Geopolymer is a novel type of aluminosilicate cementitious material, which is rapidly gaining more and more attention due to its high engineering performance[4] and low carbon footprint[5]. During the geopolymer production, industrial solid wastes, such as metakaolin[6], fly ash[7] and red mud[8], are usually adopted as the precursors of alkali-activated reactions. Meanwhile, the geopolymer production can be carried out at room temperature and pressure, which greatly reduces the energy consumption and CO_2 emissions of geopolymer production. It has been reported that the CO_2 emission during the geopolymer production is nearly 90% lower than that of the ordinary Portland cement[9], which demonstrates the outstanding environmentally friendly characteristic of geopolymer. Moreover, because of the unique three-dimensional mesh structures connected by Si-O-T bonds, geopolymer also exhibits satisfactory compressive strength[10] and remarkable thermal stability[11]. As a result, geopolymer is widely regarded as the most promising alternative to cement.

1.2. Review on the toughness of geopolymer-based composites

Although geopolymer presents some outstanding properties, its low toughness behavior under bending loads greatly limits its engineering applications. Specifically, Pan et al. have pointed out that for the cement and geopolymer specimens with the same compressive strength level, the toughness of geopolymer specimen is found to be only 30% of that exhibited by the cement specimen [12]. Therefore, adopting various approaches to enhance the toughness of geopolymer composites has become a key issue in the geopolymer research.

Fiber and nanoparticle modifications are widely employed methods to enhance the toughness of geopolymer composites. Recent reports point out that various types of fibers, such as carbon fibers[13], steel fibers[14] and PVA fibers[15], can graetly enhance the toughness of geopolymer matrix by virtue of their high toughness. Specifically, these fibers play a crucial role in inhibiting crack development within the geopolymer matrix by absorbing damage energy during the flexural failure of geopolymer composites via fiber pull-out and fiber breakage effects[16]. Furthermore, the addition of nanoparticles primarily promotes the formation of reaction products by providing nucleation sites for geopolymerizaton[17], thus enhancing the toughness of geopolymer composites. In addition, the nanoparticles can also fill the pores inside geopolymer matrix, thus improving its resistance to bending deformation by enhancing the compactness[18]. However, when the fiber or nanoparticle content within geopolymer matrix exceeds a certain threshold, the anisotropism within geopolymer composites will be intensified[19,20], which in turn reduces the mechanical properties of geopolymer composites, thus limiting the toughening effect of fibers and nanoparticles on the geopolymer matrix.

In order to avoid the hazards associated with the aggregation of toughening fillers within geopolymer matrix, epoxy resin that can exhibit strong compatibility and coupling with inorganic cementitious materials[21,22] have been adopted in some literatures to enhance the toughness of geopolymer composites[23]. According to Xiong et al., the geopolymer containing 4 wt% epoxy resin presents both good compressive and flexural strengths[24]. This may be mainly attributed to the formation of hydrogen bonds between epoxy resin and geopolymer products[25], which allows the epoxy resin with a high toughness to be embedded inside the geopolymer matrix, thus improving the ductility of geopolymer. However, although epoxy resin can be well compatible with geopolymer matrix, epoxy resin is also highly susceptible to brittle fracture at low temperatures[26]. Therefore, polyurethane with a better flexibility can be considered to modify the epoxy resin, thus further enhancing the toughness of geopolymer matrix on the basis of ensuring the compatibility of organic emulsion with geopolymer matrix. However, there are few reports on the co-modification mechanism of epoxy resin and polyurethane on the geopolymer composites, which is the focus of this work.

1.3. Aims and organization of this study

This work aims to enhance the toughness of metakaolin-based geopolymer matrix with polyurethane and E44 epoxy resin, thereby improving the potential of geopolymer to replace cement. Then, the co-toughening mechanism of polyurethane and epoxy resin on the metakaolin-based geopolymer matrix was revealed by analyzing the changes of chemical bonds inside the geopolymer composites before and after modification so as to provide theoretical guidance for the practical engineering applications of geopolymer composites.

2. Methodology

2.1. Raw materials

E44 epoxy resin, waterborne polyurethane, dibutyltin dilaurate (DBTDL) and triethylene tetramine were provided by Macklin Co., Ltd. The solid content of E44 epoxy resin and waterborne polyurethane is 50 wt% and 40 wt%, respectively. Metakaolin (MK), silica fume (SF) and granulated blast furnace slag (GBFS) were served as the aluminosilicate precursors for the preparation of geopolymer

Table 1
Primary chemical components of MK, GBFS and SF.

Materials	SiO_2	Al_2O_3	CaO	Fe_2O_3	MgO	Na_2O	K_2O	SO_3	Others
MK	53.89	42.83	0.11	0.77	0.06	0.01	0.07	0.14	2.12
GBFS	26.44	13.14	48.52	0.32	5.35	0.49	0.31	4.41	1.02
SF	96.92	0.52	1.03	0.09	0.31	0.18	0.61	0.17	0.17

matrix. The primary chemical components of MK, GBFS and SF are shown in Table 1.

Fig. 1 presents the X-ray diffraction (XRD) spectra of MK, SF and GBFS. The purity of NaOH is higher than 97%. The water glass is a yellowish transparent liquid with a modulus of 3.3, and its SiO_2 and Na_2O contents are 27.3 wt% and 8.54 wt%, respectively.

2.2. Specimen preparation

2.2.1. Preparation of polyurethane modified epoxy resin and EP

E44 epoxy resin, polyurethane prepolymer and DBTDL were added into a three-neck flask sequentially, following by a 30-minute stirring. DBTDL played a role of catalyst in this chemical reaction. Then the −N = C═O group content of the composite emulsion was measured every 15 min until it approached to 0, which signified the completion of the substitution reaction. Subsequently, a 30 min of vacuum defoaming was conducted to yield the polyurethane modified epoxy resin (PMER). The synthesis process of PMER is illustrated in Fig. 2.

Then, epoxy resin and PMER were poured into a flask and cured by triethylene tetramine to produce the EP. Triethylene tetramine can break the epoxy ring of epoxy resin molecule, thus forming hydroxyl groups at both ends of the epoxy resin chain. Fig. 3 typically shows the curing process of PMER, which can representatively reflect the preparation process of EP.

2.2.2. Preparation of EMG specimens

Prior to preparing EMG specimens, a composite alkali activator with a modulus of 1.2 was created by mixing NaOH and water glass in a mass ratio of 1:5. The concentration of the composite alkali activator is 42.58 wt%. Since the dissolution of NaOH in water glass released a large amount of heat, the evaporated water was replenished after the composite alkali activator was cooled to the room temperature. Then, MK, SF, GBFS, composite alkali activator, and fresh EP emulsion were mixed and stirred uniformly in a stirring pot to obtain the EMG paste. Finally, the EMG paste was injected into molds and maintained at 20 °C and 95% humidity for 28 d to obtain the EMG specimens. The overall preparation process of EMG specimens is illustrated in Fig. 4.

2.3. Mix design

EP emulsions were prepared by replacing epoxy resin with different proportions of PMER. Subsequently, these EP emulsions were added into the metakaolin-based geopolymer matrix in the same dosage so as to produce EMG specimens. The specific mix design of pure metakaolin-based geopolymer and EMG specimens is presented in Table 2, where the water-solid ratio and EP emulsion dosage were fixed at 0.44 and 10 wt%, respectively.

2.4. Performance test methods

The number of parallel samples for each test was 3. The elongation at break of the cured EP was tested according to Chinese standard GB/T 2567–2021 with a loading rate of 10 mm/min. The mechanical behavior of EMG specimens was measured based on Chinese standard GB/T 17671–2021. XRD testing was adopted to characterize the crystalline phase composition of raw materials and the reaction product type of EMG specimens. During the XRD testing, the scanning speed was fixed at 1°/min. Typical functional groups of EMG specimens and cured EP were measured by fourier transform infrared spectroscopy (FTIR) testing. X-ray photoelectron spectroscopy testing were used for characterizing the geopolymerization degree of EMG specimens. The microscopic morphology of

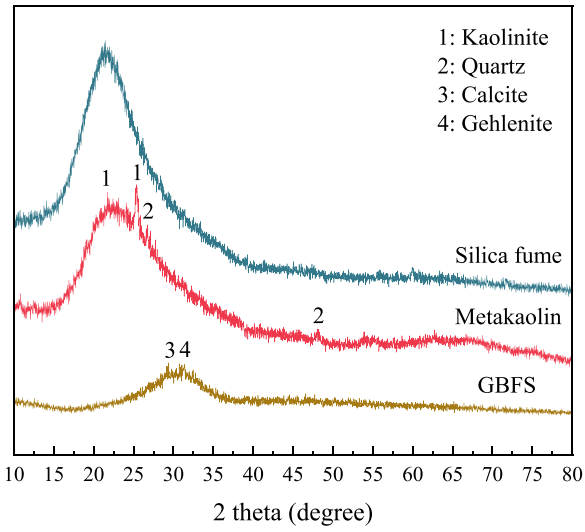

Fig. 1. XRD spectra of MK, SF and GBFS used in this study.

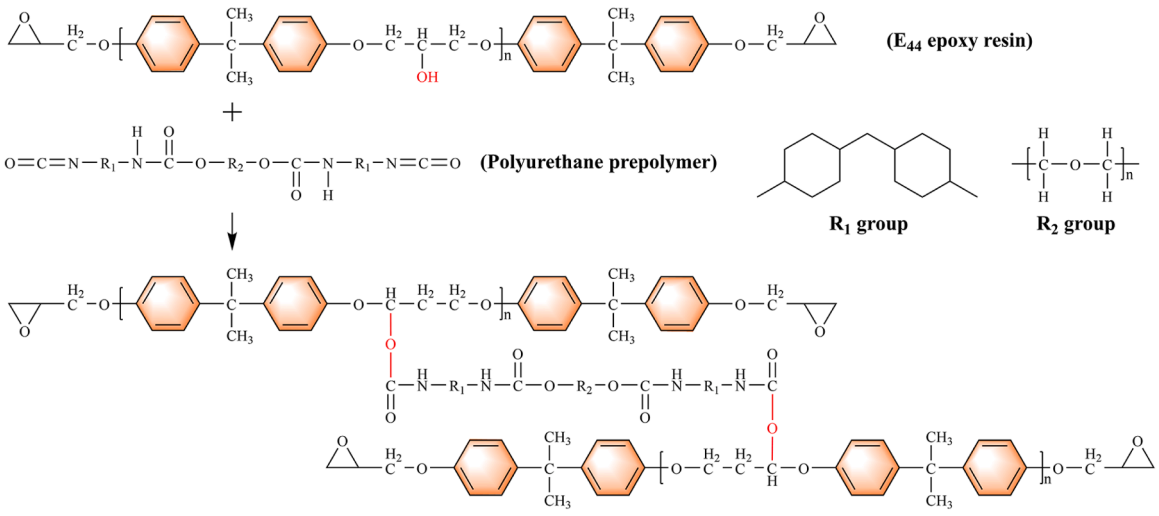

Fig. 2. Chemical reaction during the synthesis process of PMER.

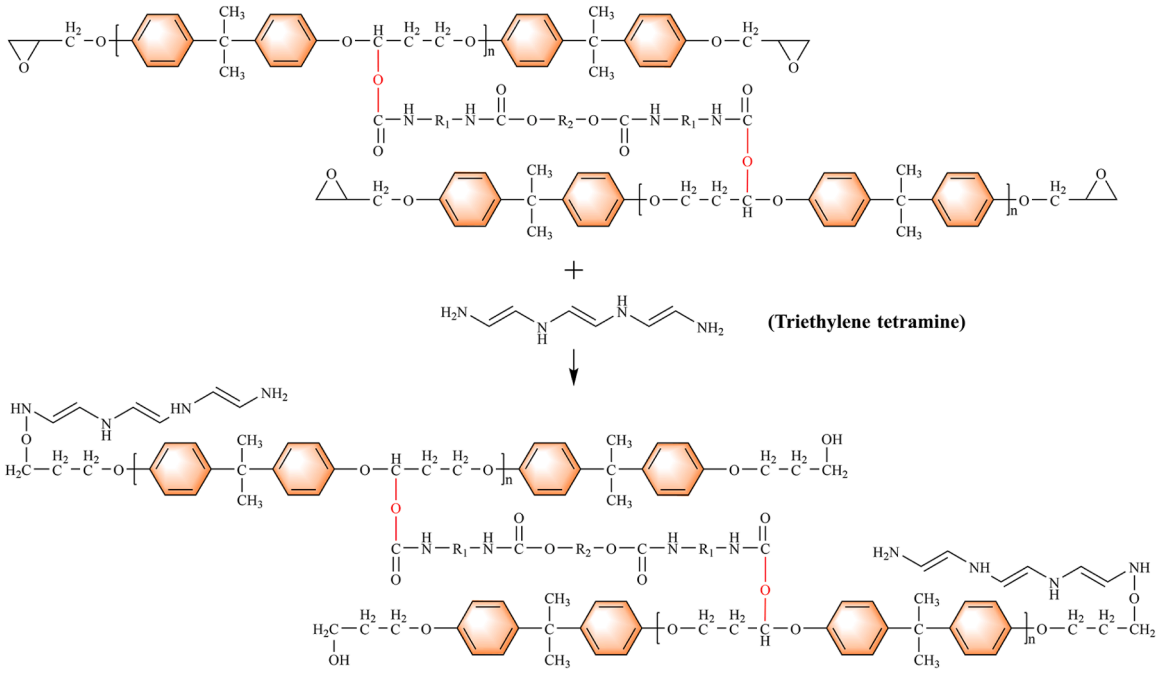

Fig. 3. Curing process of PMER.

pure metakaolin-based geopolymer and EMG specimens was observed by SEM testing.

3. Results and discussions

3.1. Toughness of cured EP with different PMER contents

Fig. 5 presents the FTIR results of cured EP specimens with different PMER replacement rates, where E40-P60 refers to the EP specimen consisting of 40 wt% epoxy resin and 60 wt% PMER. The peaks between 2830 cm^{-1} and 3100 cm^{-1} reflect the stretching vibrations of the C-H bonds in -CH_2 and -CH_3[27]. The peak near 1726 cm^{-1} is attributed to the symmetric stretching vibrations of the -COO on the polyurethane molecules[28]. The peaks around 1603 cm^{-1} and 1505 cm^{-1} are associated with the benzene rings on epoxy resin, while the peak at 910 cm^{-1} is assigned to the anhydrous rings of epoxy resin[24]. It can be seen from Fig. 5(b) that the peak intensity of -COO enhances gradually with the increase of the PMER content, which indicates that the polyurethane molecule has

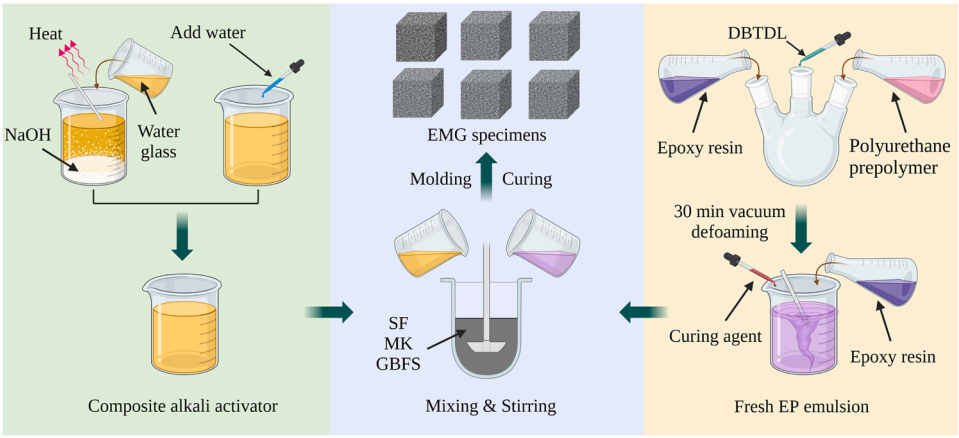

Fig. 4. Schematic diagram for the preparation process of EMG specimens.

Table 2
Specific mix design of pure metakaolin-based geopolymer and EMG specimens.

Mix	MK (g)	SF (g)	GBFS (g)	Composite alkali activator (g)	EP emulsion (g)	Epoxy resin (wt%)	PMER (wt%)
XH1	144	48	48	180	0	0	0
XH2	144	48	48	180	31.8	100	0
XH3	144	48	48	180	31.8	80	20
XH4	144	48	48	180	31.8	60	40
XH5	144	48	48	180	31.8	40	60
XH6	144	48	48	180	31.8	20	80
XH7	144	48	48	180	31.8	0	100

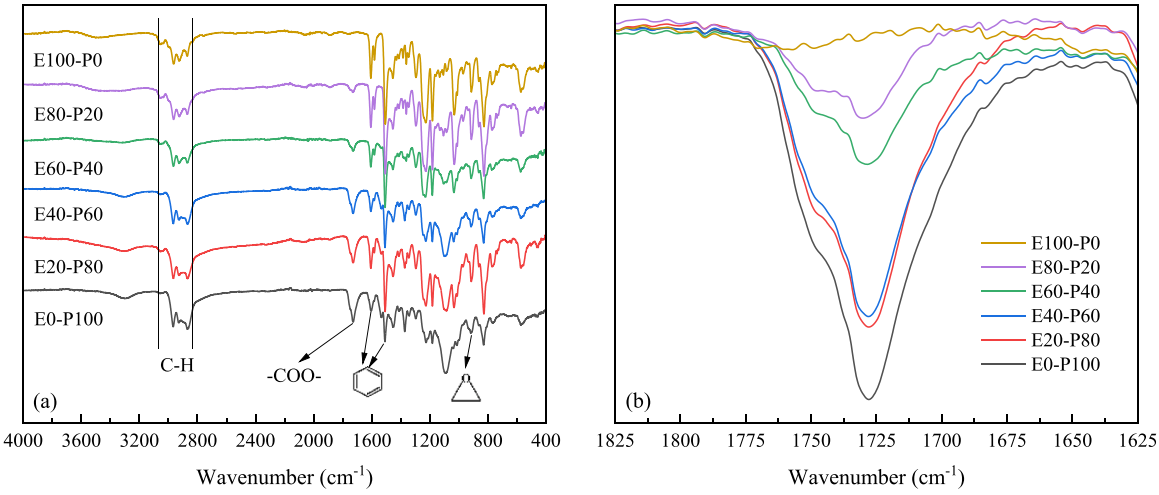

Fig. 5. FTIR results of cured EP specimens with different PMER replacement rates; (a) Full spectra; (b) Peak at 1726 cm^{-1}.

been successfully grafted onto the epoxy resin molecule.

Fig. 6 further illustrates the elongation at break of the cured EP specimens at different PMER replacement rates. As can be seen from Fig. 6, the introduction of polyurethane significantly improved the toughness of EP. Specifically, when the proportion of PMER was increased from 0 wt% to 100 wt%, the elongation at break of EP was enhanced by 6.1 times, which can be mainly attributed to the high toughness of polyurethane[29].

3.2. Mechanical behavior of EMG specimens

The 6 groups of EP emulsions shown in Section 3.1 were respectively added into metakaolin-based geopolymer matrix to prepare

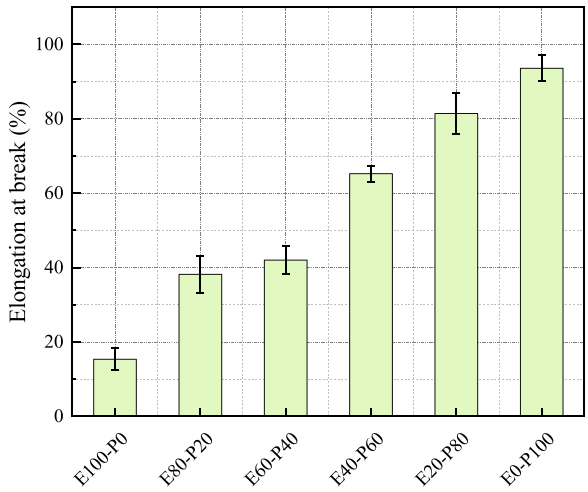

Fig. 6. Elongation at break of cured EP specimens with different PMER contents.

the EMG specimens. Fig. 7 presents the 28d flexural strength of pure metakaolin-based geopolymer and EMG specimens.

Fig. 7 clearly illustrates that as the PMER content within EP emulsion increases, the 28d flexural strength of EMG initially enhances and then shows an obvious drop trend. In particular, when the PMER content inside EP emulsion reaches 60 wt%, the 28d flexural strength of EMG achieves a peak value of 5.7 MPa, which is 2.6 times greater than that of the pure metakaolin-based geopolymer. In addition, it is worth mentioning that the EMG specimens consistently present a higher 28d flexural strength than that of the pure metakaolin-based geopolymer specimen, regardless of the PMER content within EP emulsion.

The increasing trend of the 28d flexural strength of EMG can be primarily attributed to the high fracture toughness of cured EP, which is also demonstrated in Fig. 6. In addition, hydrogen bonds can be generated between EP molecules and the Si-O-Al structures within metakaolin-based geopolymer matrix[30], which can help forming a larger 3D mesh structure inside the EMG, thus enhancing its toughness. The formation of hydrogen bonds within EMG is schematically illustrated in Fig. 8. However, Fig. 6 also reveals that since the brittleness of epoxy resin is higher than that PMER, the elongation at break of cured EP continues to increase as the PMER content enhances. As a result, the decreasing trend in the 28d flexural strength of EMG shown in Fig. 7 may be attributed to some special chemical reactions between EP molecules and the geopolymer matrix, which affects the geopolymerization degree of EMG, thus weakening its toughness.

The XRD spectra of pure metakaolin-based geopolymer and EMG specimens are illustrated in Fig. 9, which shows that all XRD spectra present a prominent amorphous dispersion peak in the range of 23° to 36°. Furthermore, these amorphous dispersion peaks display a noticeable rightward shift in comparison to those of the raw materials shown in Fig. 1, which indicates that the geopolymerization has occurred within pure metakaolin-based geopolymer and EMG. In addition, Fig. 9 also indicates that the pure metakaolin-based geopolymer and EMG present the same crystal type, which suggests that the evolution in the 28d flexural strength of EMG after the addition of EP is not caused by the introduction of new products. Meanwhile, the amorphous dispersion peak of the EMG shows a rightward shift compared with that of the pure metakaolin-based geopolymer, which implies that EP may promote the

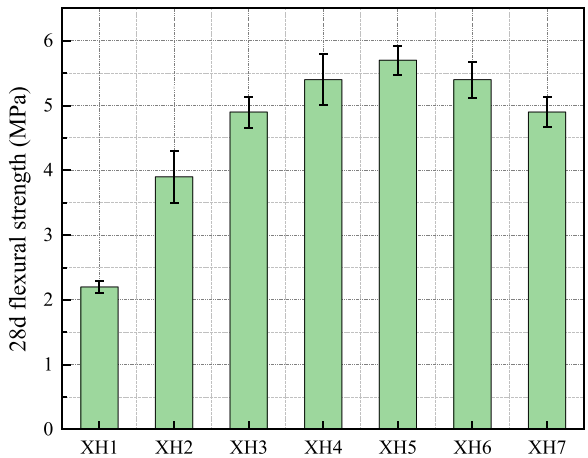

Fig. 7. 28d flexural strength of pure metakaolin-based geopolymer specimen and EMG specimens with different PMER contents.

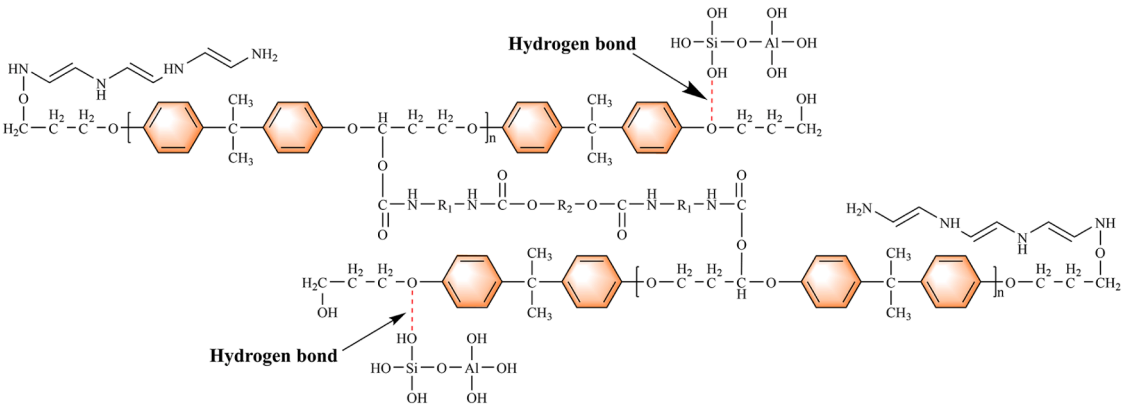

Fig. 8. Schematic diagram of the hydrogen bond formation within EMG specimens.

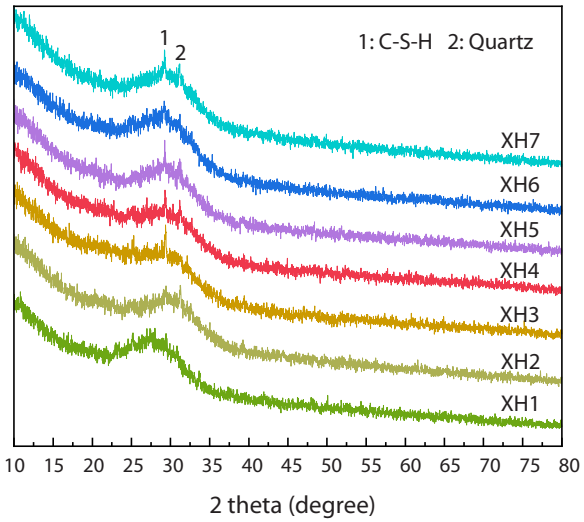

Fig. 9. XRD spectra of pure metakaolin-based geopolymer specimen and EMG specimens with different PMER contents.

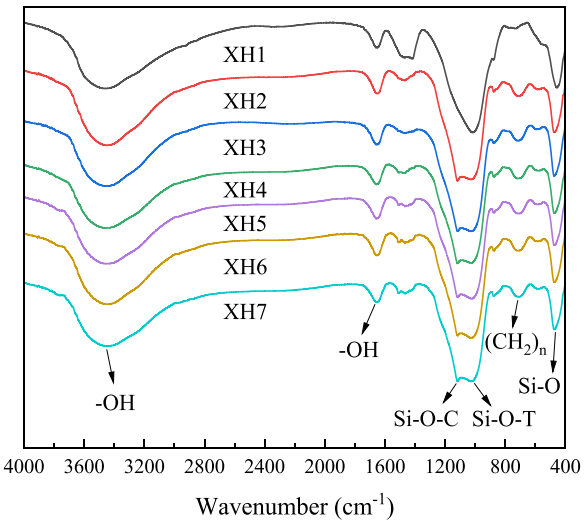

Fig. 10. FTIR results of pure metakaolin-based geopolymer specimen and EMG specimens with various PMER contents.

geopolymerization within metakaolin-based geopolymer matrix. Meanwhile, a slight leftward shift of the amorphous dispersion peak is observed in the XRD spectra of EMG specimens as the PMER content increases. It indicates that the drop trend for the 28 d flexural strength of EMG shown in Fig. 7 may be mainly attributed to the decrease of geopolymerization degree of EMG.

Hence, FTIR tests were conducted to further observe the evolution of major functional groups within the pure metakaolin-based geopolymer and EMG specimens. Fig. 10 presents the FTIR spectra, where the peaks at 3451 cm^{-1} and 1654 cm^{-1} are respectively caused by the asymmetric stretching and bending vibrations of the O-H bond[31]. In addition, the peak near 713 cm^{-1} is associated with coupling vibrations between the multiple -CH_2 groups of EP molecules[32], while the peak around 464 cm^{-1} can be assigned to the bending vibration of Si-O bonds[33]. It is worth pointing out that the peak at 1004 cm^{-1} is attributed to the asymmetric stretching vibration of the Si-O-T (T represents Si or Al) bonds within geopolymer gels, and its peak intensity is proportional to the amount of geopolymer gels[34]. Therefore, the area of the peak at 1004 cm^{-1} was calculated via OMNIC software and the results are shown in Table 3.

Combining Fig. 10 and Table 3, EMG specimens present a greater Si-O-T peak area than that of the pure metakaolin-based geopolymer. Meanwhile, the Si-O-T peak intensity of EMG shows a drop trend as the PMER content increases. It implies that in addition to the hydrogen bonding, EP molecules can interact with the silica-alumina oligomers within geopolymer matrix via other pattern, thereby affecting the formation of Si-O-T structures and the evolution of EMG flexural strength. Specifically, comparing with the FTIR spectrum of pure metakaolin-based geopolymer specimen (XH1), a peak corresponding to the stretching vibration of the Si-O-C bond at 1123 cm^{-1} can be observed in the FTIR spectra of EMG specimens[35]. It indicates that the $Si(OH)_4$ or Si-O-T within geopolymer matrix has reacted with the -OH groups on the EP molecules under an alkaline condition, which may influence the toughness of EMG.

3.3. Reaction mechanism between EP and geopolymer products

Based on the above analysis, XPS tests were further adopted to characterize the geopolymerization degree of EMG specimens at different PMER contents. Fig. 11 shows the Si 2p high-resolution spectra of EMG specimens. The Si 2p spectrum can be primarily divided into the following three peaks. The peak around 101.3 eV represents the Si-O-T bonds within geopolymer gels[16]. The peak at 102.2 eV is associated with the non-bridging oxygen, while the peak caused by the Si-O-C bond is near 103.2 eV[36]. As can be seen from Fig. 11, obvious Si-O-C peaks can be found in the Si 2p high-resolution spectra of all EMG specimens, and the specific area proportion of each peak in the Si 2p high-resolution spectra is calculated in Table 4. As can be seen form Fig. 11 and Table 4, the area proportion of Si-O-T and Si-O-C peaks present a clear drop trend as the PMER content within EMG increases, which is opposite to that of the Si-OH peak. It suggests that the increasing PMER content within EP emulsion can reduce the geopolymerization degree of EMG by weakening the reaction between EP molecules and geopolymer products, which in turn adversely affects the toughness of EMG.

In detail, the active aluminosilicates in raw materials will dissolve under the contribution of composite alkali activator to generate $Si(OH)_4$ and $[Al(OH)_4]^-$ monomers. These monomers, once generated, promptly undergo polymerization in the alkali environment, leading to the production of Si-O-T structures[37]. Therefore, both $Si(OH)_4$ and Si-O-T structures were present within MEG before the end of geopolymerization. Significantly, the -OH groups on PMER and epoxy resin molecules can react with $Si(OH)_4$ monomer and Si-O-T oligomers under the alkali condition, which in turn connects the geopolymer gels with EP molecules into a larger 3D mesh structure through Si-O-C bonding, thus contributing to the toughness enhancement of EMG. In addition, the chemical adsorption of EP molecules to $Si(OH)_4$ monomers also reduces the contacting difficulty between $Si(OH)_4$ monomers, thus intensifying the polymerization of $Si(OH)_4$ monomers to form Si-O-Si structures, which is beneficial.

for enhancing the flexural strength of EMG. Specific reaction schematics are shown in Figs. 12 and 13. However, Fig. 2 clearly illustrates that PMER was synthesized through the bonding of polyurethane with the -OH groups on the epoxy resin. As a result, the increase of PMER dosage reduces the -OH group content of EP emulsion, which in turn weakens the adsorption potential of EP molecules towards $Si(OH)_4$ and Si-O-T structures in the alkali environment. Therefore, as the PMER content of EP emulsion increases, the geopolymerization degree of EMG diminishes, which adversely affects its toughness development.

Overall, although the increase of PMER content contributes to the toughness improvement of EMG by enhancing the elongation at break of EP, it also reduces the -OH group content of EP, which in turn weakens the geopolymerization degree of EMG, thus resulting in an adverse effect on the toughness improvement of EMG. When the PMER content in the EP emulsion exceeds 60 wt%, the impact of decreased geopolymerization degree on the toughness of EMG becomes evident, thus leading to a drop in the 28d flexural strength of EMG shown in Fig. 7. However, the toughness of EMG is always higher than that of the pure metakaolin-based geopolymer regardless of the variation of PMER content within EP emulsion, which can be mainly attributed to the presence of -OH on the cured E0-P100 molecules. Fig. 14 further supported the above analysis, which clearly presents that the geopolymer gels within the pure metakaolin-based geopolymer (XH1 specimen) is loosely distributed, which is not conducive to the development of strength[38,39], thus leading to a low flexural strength. In contrast, the geopolymer gel phase within the EMG specimen modified with E100-P0 emulsion (XH2 specimen) is denser and the connection between EP and geopolymer gels is obviously tight. As the proportion of PMER within EP increases, the geopolymerization degree gradually decreases, which results in the poor bonding of different phases in EMG, thus in turn causing to cracks and pores inside EMG specimens.

4. Conclusions

In this work, the toughness of metakaolin-based geopolymer was enhanced using the EP emulsion composed of PMER and epoxy resin. In addition, the co-toughening mechanism of polyurethane and epoxy resin on the metakaolin-based geopolymer matrix was revealed from the perspective of chemical bond variation, which contributes to a better understanding of the mechanical behavior of

Table 3
Area of the peak at 1004 cm^{-1}.

Mixture	XH1	XH2	XH3	XH4	XH5	XH6	XH7
Peak area (A.U.)	3452	4657	4525	4323	4155	4054	3907

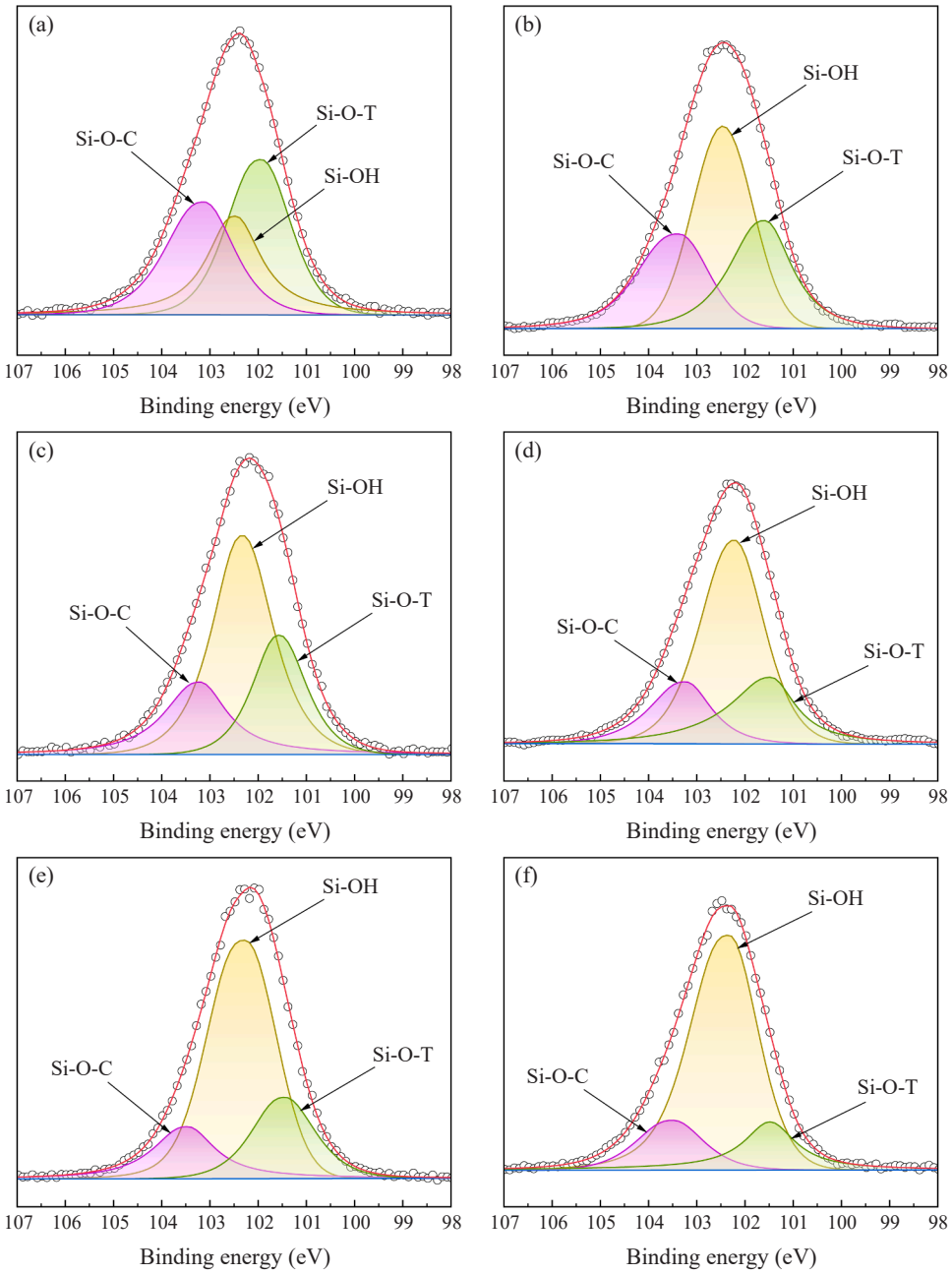

Fig. 11. Si 2p high-resolution spectra of EMG specimens modified by (a) E100-P0 emulsion (b) E80-P20 emulsion; (c) E60-P40 emulsion; (d) E40-P60 emulsion; (e) E20-P80 emulsion; (f) E0-P100 emulsion.

geopolymer composites. Based on the experimental results, the following conclusions can be obtained.

(1)The introduction of polyurethane can significantly enhance the elongation at break of cured EP, which in turn contributes to the toughness enhancement of EMG. Moreover, -OH groups on EP molecules can form Si-O-C bonds with Si-O-T oligomers and $Si(OH)_4$ monomers within geopolymer matrix, which further promotes the cross-linking between multiple 3D mesh structures inside EMG, thus

Table 4
Area proportion of each peak in the Si 2p high-resolution spectra of EMG specimens.

Peak	Fig. 11 (a)	Fig. 11 (b)	Fig. 11 (c)	Fig. 11 (d)	Fig. 11 (e)	Fig. 11 (f)
Si-O-T (%)	39.62	27.81	24.98	24.36	20.52	15.62
Si-OH (%)	28.31	45.58	53.01	57.84	63.14	69.97
Si-O-C (%)	32.07	26.61	22.01	17.80	16.34	14.41

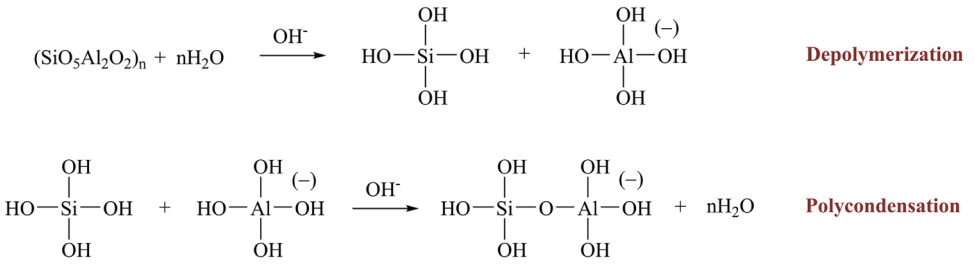

Fig. 12. Depolymerization and polycondensation processes in geopolymerization.

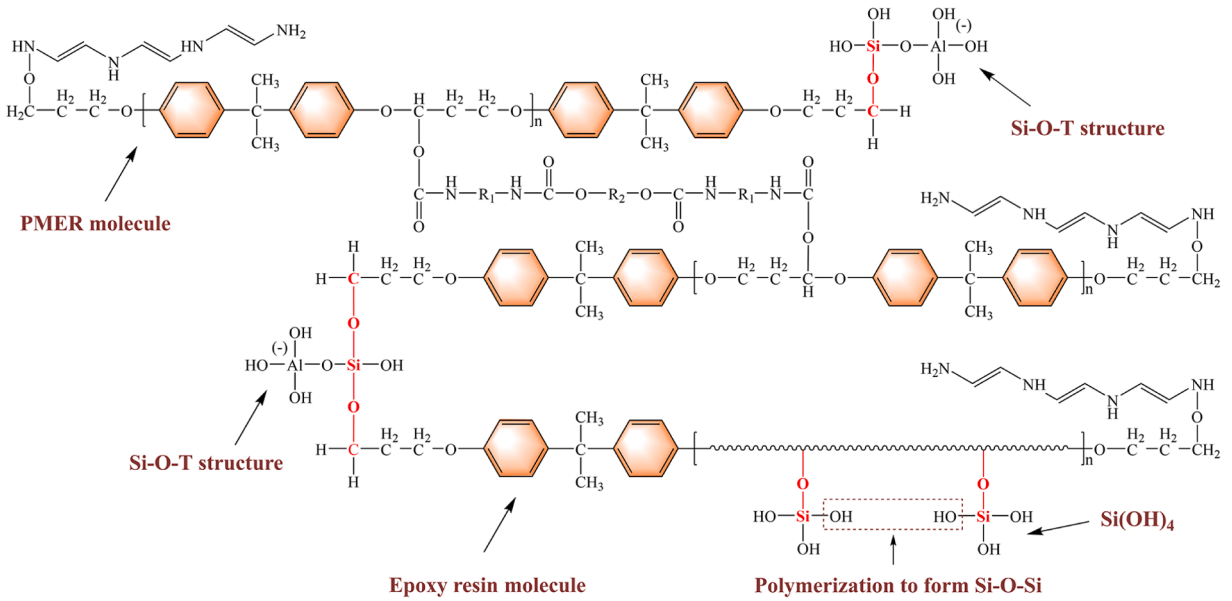

Fig. 13. Schematic diagram for the modification mechanism of EP on metakaolin-based geopolymer matrix.

enhancing the toughness of EMG.

(2)The increase of PMER content decreases the -OH content in the EP emulsion, which inhibits the formation of Si-O-C bonds inside EMG, thus weakening the geopolymerization degree of EMG. When the PMER content within EP emulsion exceeds 60 wt%, the weakening effect of PMER on the geopolymerization of EMG begins to dominate, resulting in a decrease in the 28d flexural strength of EMG with increasing PMER content inside EP emulsion.

(3)The 28d flexural strength of EMG specimen toughened with 10 wt% EP emulsion (containing 60 wt% PMER) can reach 5.7 MPa, which is 2.6 times greater than that of the pure metakaolin-based geopolymer specimen.

(4)Regardless of the PMER content in EP emulsion, the EMG specimens consistently presents a higher 28d flexural strength compared to the pure metakaolin-based geopolymer. This can be mainly attributed to the high fracture toughness of the cured EP, the hydrogen bonds between Si-O-T structures and EP molecules, and the intrinsic -OH in the tail chain of PMER molecules.

CRediT authorship contribution statement

Chen Feng: Data curation, Investigation, Validation. **Ma Tao:** Conceptualization, Funding acquisition, Investigation, Project administration. **Gu Gonghui:** Data curation, Formal analysis, Methodology, Writing – original draft. **Xu Fang:** Data curation,

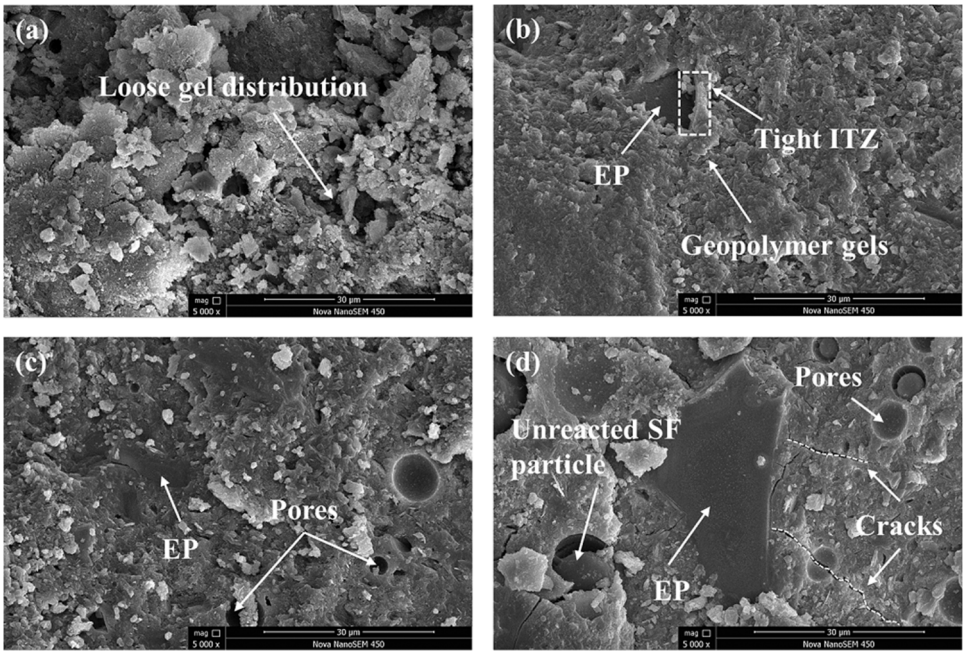

Fig. 14. Micromorphology of pure metakaolin-based geopolymer and typical EMG specimens; (a) XH1 specimen; (b) XH2 specimen; (c) XH5 specimen; (d) XH7 specimen.

Validation. **Shi Yingqi:** Investigation, Validation, Writing – review & editing.

Declaration of Competing Interest

The authors declare that they have no known competing financial interests or personal relationships that could have appeared to influence the work reported in this paper.

Data availability

Data will be made available on request.

Acknowledgements

This work was supported by National Key Research and Development Project of China (2020YFB1600102), National Natural Science Foundation of China (51922030; 52208430), Natural Science Foundation of Jiangsu Province (BK20210248), Shuangchuang Program of Jiangsu Province (JSSCBS20210058), and China Scholarship Council.

References

[1] Q. Munir, M. Abdulkareem, M. Horttanainen, T. Kärki, A comparative cradle-to-gate life cycle assessment of geopolymer concrete produced from industrial side streams in comparison with traditional concrete, Sci. Total Environ. 865 (2023) 161230, https://doi.org/10.1016/j.scitotenv.2022.161230.
[2] Y.I.A. Aisheh, D.S. Atrushi, M.H. Akeed, S. Qaidi, B.A. Tayeh, Influence of polypropylene and steel fibers on the mechanical properties of ultra-high-performance fiber-reinforced geopolymer concrete, Case Stud. Constr. Mat. 17 (2022) e01234, https://doi.org/10.1016/j.cscm.2022.e01234.
[3] Z. Gao, Y. Li, H. Qian, M. Wei, Environmental, economic, and social sustainability assessment: a case of using contaminated tailings stabilized by waste-based geopolymer as road base, Sci. Total Environ. 888 (2023) 164092, https://doi.org/10.1016/j.scitotenv.2023.164092.
[4] J. Shang, J. Dai, T. Zhao, S. Guo, P. Zhang, B. Mu, Alternation of traditional cement mortars using fly ash-based geopolymer mortars modified by slag, J. Clean. Prod. 203 (2018) 746–756, https://doi.org/10.1016/j.jclepro.2018.08.255.
[5] Y.A. Al-Noaimat, S.H. Ghaffar, M. Chougan, M.J. Al-Kheetan, A review of 3D printing low-carbon concrete with one-part geopolymer: engineering, environmental and economic feasibility, Case Stud. Constr. Mat. 18 (2023) e01818, https://doi.org/10.1016/j.cscm.2022.e01818.
[6] J. Han, J. Pan, X. Wang, J. Cai, L. Gu, J. Yang, Conductive behavior of engineered geopolymer composite with addition of carbon fiber and nano-carbon black, Ceram. Int 49 (2023) 32035–32048, https://doi.org/10.1016/j.ceramint.2023.07.170.
[7] G. Gu, T. Ma, F. Chen, C. Han, H. Li, F. Xu, Controlling electromagnetic and mechanical behaviors of geopolymer matrix with nano-SiO2@Fe3O4 magnetofluid for soft magnetic applications, Cem. Concr. Compos. 145 (2024) 105370, https://doi.org/10.1016/j.cemconcomp.2023.105370.
[8] X. Wan, J. Ding, N. Jiao, C. Mou, M. Gao, Mechanical and microstructural properties of cement-treated marine dredged clay with red mud and phosphogypsum, B Eng. Geol. Environ. 81 (2022) 266, https://doi.org/10.1007/s10064-022-02753-5.
[9] J. Tan, H. Dan, Z. Ma, Metakaolin based geopolymer mortar as concrete repairs: bond strength and degradation when subjected to aggressive environments, Ceram. Int 48 (2022) 23559–23570, https://doi.org/10.1016/j.ceramint.2022.05.004.

[10] T. Kovářík, J. Hájek, M. Pola, D. Rieger, M. Svoboda, J. Beneš, P. Šutta, K. Deshmukh, V. Jandová, Cellular ceramic foam derived from potassium-based geopolymer composite: thermal, mechanical and structural properties, Mater. Des. 198 (2021) 109355, https://doi.org/10.1016/j.matdes.2020.109355.
[11] F. Matalkah, A. Ababneh, R. Aqel, Synthesis of calcined kaolin-based geopolymer foam: assessment of mechanical properties, thermal insulation, and elevated temperature stability, Ceram. Int 49 (2023) 9967–9977, https://doi.org/10.1016/j.ceramint.2022.11.174.
[12] Z. Pan, J.G. Sanjayan, B.V. Rangan, Fracture properties of geopolymer paste and concrete, Mag. Concr. Res 63 (2011) 763–771, https://doi.org/10.1680/macr.2011.63.10.763.
[13] G. Gu, T. Ma, F. Chen, C. Han, H. Li, F. Xu, Co-modifying geopolymer composite by nano carbon black and carbon fibers to reduce CO_2 emissions in airport pavement induction heating, Compos. Part a: Appl. Sci. Manuf. 177 (2024) 107951, https://doi.org/10.1016/j.compositesa.2023.107951.
[14] R.R. Bellum, Influence of steel and PP fibers on mechanical and microstructural properties of fly ash-GGBFS based geopolymer composites, Ceram. Int 48 (2022) 6808–6818, https://doi.org/10.1016/j.ceramint.2021.11.232.
[15] H.H. Nguyễn, P.H. Nguyễn, Q. Lương, W. Meng, B.Y. Lee, Mechanical and autogenous healing properties of high-strength and ultra-ductility engineered geopolymer composites reinforced by PE-PVA hybrid fibers, Cem. Concr. Compos. 142 (2023) 105155, https://doi.org/10.1016/j.cemconcomp.2023.105155.
[16] G. Gu, Y. Pei, T. Ma, F. Chen, J. Zhang, F. Xu, Role of carbon fiber in the electrothermal behavior and geopolymerization process of carbon fiber-reinforced FA-GBFS geopolymer composite, Constr. Build. Mater. 369 (2023) 130597, https://doi.org/10.1016/j.conbuildmat.2023.130597.
[17] A.S. Rahman, P. Jackson, D.W. Radford, Improved toughness and delamination resistance in continuous fiber reinforced geopolymer composites via incorporation of nano-fillers, Cem. Concr. Compos. 108 (2020) 103496, https://doi.org/10.1016/j.cemconcomp.2019.103496.
[18] T. Alomayri, A. Raza, F. Shaikh, Effect of nano SiO2 on mechanical properties of micro-steel fibers reinforced geopolymer composites, Ceram. Int 47 (2021) 33444–33453, https://doi.org/10.1016/j.ceramint.2021.08.251.
[19] H. Zhong, M. Zhang, Engineered geopolymer composites: a state-of-the-art review, Cem. Concr. Compos. 135 (2023) 104850, https://doi.org/10.1016/j.cemconcomp.2022.104850.
[20] J. Han, J. Pan, J. Cai, X. Li, A review on carbon-based self-sensing cementitious composites, Constr. Build. Mater. 265 (2020) 120764, https://doi.org/10.1016/j.conbuildmat.2020.120764.
[21] Y. Li, H. Guan, Y. Bao, S. Guo, D. Lei, T. Zhao, B. Zhong, Z. Li, Ni0.6Zn0.4Fe2O4/Ti3C2Tx nanocomposite modified epoxy resin coating for improved microwave absorption and impermeability on cement mortar, Constr. Build. Mater. 310 (2021) 125213, https://doi.org/10.1016/j.conbuildmat.2021.125213.
[22] Y. Bao, S. Guo, Z. Jia, H. Guan, Effects of MOFs-derived Ni@NC/CNT nanocomposites on impermeability and microwave absorption of modified epoxy resin coatings on cement-based materials, Constr. Build. Mater. 383 (2023) 131337, https://doi.org/10.1016/j.conbuildmat.2023.131337.
[23] A. Saludung, Y. Ogawa, K. Kawai, Microstructure and mechanical properties of epoxy resin-reinforced geopolymer exposed to high temperatures, Mater. Lett. 331 (2023) 133473, https://doi.org/10.1016/j.matlet.2022.133473.
[24] G. Xiong, X. Guo, H. Zhang, Preparation of epoxy resin-geopolymer (ERG) for repairing and the microstructures of the new-to-old interface, Compos. Part B: Eng. 259 (2023) 110731, https://doi.org/10.1016/j.compositesb.2023.110731.
[25] J. Ren, S. Guo, J. Su, T. Zhao, J. Chen, S. Zhang, A novel TiO2/Epoxy resin composited geopolymer with great durability in wetting-drying and phosphoric acid solution, J. Clean. Prod. 227 (2019) 849–860, https://doi.org/10.1016/j.jclepro.2019.04.203.
[26] Q. He, H. Zhang, J. Li, H. Duan, Performance evaluation of polyurethane/epoxy resin modified asphalt as adhesive layer material for steel-UHPC composite bridge deck pavements, Constr. Build. Mater. 291 (2021) 123364, https://doi.org/10.1016/j.conbuildmat.2021.123364.
[27] D. Wang, L. Xuan, G. Han, A.H.H. Wong, Q. Wang, W. Cheng, Preparation and characterization of foamed wheat straw fiber/polypropylene composites based on modified nano-TiO2 particles, Compos. Part a: Appl. Sci. Manuf. 128 (2020) 105674, https://doi.org/10.1016/j.compositesa.2019.105674.
[28] Y. Liu, Q. Lin, J. Chen, Y. Shao, Y. Wang, J. Wang, PDMS-OH and nano-SiO2 Modified KH570-TEOS silica-sol coating and protective effect on concrete, Colloids Surf. a: Physicochem. Eng. Asp. 648 (2022) 129279, https://doi.org/10.1016/j.colsurfa.2022.129279.
[29] K. Wei, Y. Wu, X. Cao, X. Yang, B. Tang, B. Shan, Dual dynamic bonds approach for polyurethane recycling and self-healing of emulsified asphalt, Sci. Total Environ. 885 (2023) 163915, https://doi.org/10.1016/j.scitotenv.2023.163915.
[30] M. Zhang, H. Xu, A.L.P. Zeze, J. Zhang, Metakaolin-based geopolymer composites modified by epoxy resin and silane: Mechanical properties and organic-inorganic interaction mechanism, Appl. Clay Sci. 232 (2023) 106767, https://doi.org/10.1016/j.clay.2022.106767.
[31] X.Q. Qi, S.L. Zhang, T.T. Wang, S.Y. Guo, R. Ren, Effect of high-dispersible graphene on the strength and durability of cement mortars, Materials 14 (2021) 915, https://doi.org/10.3390/ma14040915.
[32] W. Xia, Y. Mao, G. Xie, Y. Peng, Role of sodium oleate in the in-situ pore wetting of porous active carbon by 1H LF NMR: implications for porous mineral flotation, Powder Technol. 392 (2021) 116–122, https://doi.org/10.1016/j.powtec.2021.07.011.
[33] G. Gu, T. Ma, F. Chen, F. Xu, J. Zhang, Electromagnetic and mechanical properties of FA-GBFS geopolymer composite used for induction heating of airport pavement, Cem. Concr. Compos. 129 (2022) 104503, https://doi.org/10.1016/j.cemconcomp.2022.104503.
[34] L. Li, Z. Ma, X. Ming, Multiscale ab-initio modeling and experiment of nano-CaCO3 and fiber synergy on toughening low-carbon geopolymer composites, Mater. Des. 233 (2023) 112280, https://doi.org/10.1016/j.matdes.2023.112280.
[35] Q. Zhang, J. Jiang, F. Gao, G. Zhang, X. Zhan, F. Chen, Engineering high-effective antifouling polyether sulfone membrane with P(PEG-PDMS-KH570)@SiO2 nanocomposite via in-situ sol-gel process, Chem. Eng. J. 321 (2017) 412–423, https://doi.org/10.1016/j.cej.2017.03.105.
[36] H. Li, R. Wang, H. Hu, W. Liu, Surface modification of self-healing poly(urea-formaldehyde) microcapsules using silane-coupling agent, Appl. Surf. Sci. 255 (2008) 1894–1900, https://doi.org/10.1016/j.apsusc.2008.06.170.
[37] F. Ates, K.T. Park, K.W. Kim, B. Woo, H.G. Kim, Effects of treated biomass wood fly ash as a partial substitute for fly ash in a geopolymer mortar system, Constr. Build. Mater. 376 (2023) 131063, https://doi.org/10.1016/j.conbuildmat.2023.131063.
[38] X. Wan, J. Ding, J. Wang, P. Gao, X. Wei, Evolution in macro-micro properties of cement-treated clay with changing ratio of red mud to phosphogypsum, Constr. Build. Mater. 392 (2023) 131972, https://doi.org/10.1016/j.conbuildmat.2023.131972.
[39] X. Wan, J. Ding, N. Jiao, S. Zhang, J. Wang, C. Guo, Preparing controlled low strength materials (CLSM) using excavated waste soils with polycarboxylate superplasticizer, Environ. Earth Sci. 82 (2023) 1–10, https://doi.org/10.1007/s12665-023-10884-5.